

See discussions, stats, and author profiles for this publication at: <https://www.researchgate.net/publication/235780018>

Polymer Crystallinity and Transport Properties at the Poly(3-hexylthiophene)/Zinc Oxide Interface

ARTICLE in THE JOURNAL OF PHYSICAL CHEMISTRY C · MAY 2011

Impact Factor: 4.77 · DOI: 10.1021/jp201343s

CITATIONS

26

READS

36

5 AUTHORS, INCLUDING:



[Claudio Melis](#)

Università degli studi di Cagliari

37 PUBLICATIONS 352 CITATIONS

[SEE PROFILE](#)



[Giuliano Mallochi](#)

Italian National Research Council

62 PUBLICATIONS 756 CITATIONS

[SEE PROFILE](#)



[Alessandro Mattoni](#)

Italian National Research Council

88 PUBLICATIONS 898 CITATIONS

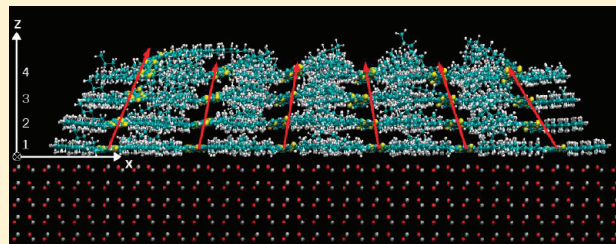
[SEE PROFILE](#)

Polymer Crystallinity and Transport Properties at the Poly(3-hexylthiophene)/Zinc Oxide Interface

Maria Ilenia Saba,^{*,†,‡} Claudio Melis,^{†,‡} Luciano Colombo,^{†,‡} Giuliano Mallochi,[‡] and Alessandro Mattoni^{*,†}

[†]Dipartimento di Fisica dell'Università di Cagliari and [‡]Istituto Officina dei Materiali del CNR, Unità SLACS, Cittadella Universitaria, I-09042 Monserrato (Ca), Italy

ABSTRACT: By means of large-scale atomistic simulations, we investigate theoretically the interface between poly(3-hexylthiophene) (P3HT) and zinc oxide. We observe a spontaneous tendency of the polymer to disorder close to the surface, and we attribute such a result to lattice spacing mismatch. By using simple effective models, we calculate the maximum polymer mobility normal to the surface that turns out to be strongly affected by the disorder at the interface. According to the present analysis, we propose that modifications of the polymer and the lattice parameter of the inorganic substrate could improve the overall transport properties at the interface.



Hybrid solar cells are attracting increasing interest due to the low cost of production and the potential of future technological developments.^{1,2} This is the case of polymer/metaloxide photovoltaic devices. In such systems, an organic conductive polymer has the role of light absorber and electron donor, while an oxide semiconductor (such as TiO₂ or ZnO) is the electron acceptor. Photogenerated hole carriers move within the organic polymer, while the electrons are collected through the inorganic component. P3HT is one of the most commonly used polymer in such hybrids because it organizes into microcrystalline domains, which gives good transport properties,^{3,4} and it provides an exciton dissociation efficiency higher than that of other conjugated polymers.⁵ As for the metaloxide, titanium dioxide (TiO₂) has been widely studied for hybrid organic–inorganic solar cells. Zinc oxide (ZnO) is an alternative that offers a very high electron mobility (200–300 cm²/V s in crystalline bulk)⁶ and high electron affinity. It is a wide-band-gap semiconductor (3.37 eV)⁶ that can be prepared in a large variety of highly ordered and highly crystalline morphologies, such as nanorods, nanotubes, nanobelts, nanorings, and many others.⁷ Hybrid P3HT/ZnO can be considered as a possible alternative to organic polymer solar cells, such as P3HT/PCBM, because, by replacing the organic acceptor with the metaloxide, it is, in principle, possible to improve the transport properties and the chemical stability of the system. Efficiencies as large as 2%⁸ have been obtained recently in P3HT/ZnO bulk heterojunction (BHJ) architectures. Such values, though very encouraging, are nevertheless much smaller than their counterpart in all organic P3HT/PCBM solar cells (around 5%). Furthermore, the power conversion efficiencies of polymer/ZnO bilayers are 1 order of magnitude smaller than that of P3HT/TiO₂ (~0.1%).¹ The above results for both bilayers and BHJ systems suggest that some fundamental issue of the P3HT/ZnO interface should be better investigated in order to further improve the performance of such a system.

Recent studies have shown that the P3HT at the interface with ZnO is rather disordered than crystalline.^{1,10} The polymer

disorder is expected to be detrimental for the efficiency of the system: for example, in the amorphous polymer, the lifetime of the carriers is shorter¹⁰ than in the crystalline case. In addition, the electronic orbital levels of P3HT and, in turn, the charge-transfer (CT) efficiency depend on the polymer crystallinity.^{1,11} Finally, better light absorption^{12,13} and transport properties are found in the crystalline polymer phase. A clear explanation for the occurrence of polymer disorder at the interface is accordingly important, and it is still missing.

In this work, by generating large-scale atomistic models of the ZnO/P3HT interface in vacuo by molecular dynamics (MD), we provide evidence that the polymer is likely disordered close to the ZnO surface, even in ideal conditions of low temperature, absence of chemical contaminants, and ideal surface. To prove this result, we analyze how the molecules stack within realistic models of interface by quantifying the unavoidable disorder induced by the surface. To study the effect of the interface microstructure on charge transport, we calculate the corresponding hole mobility by developing an effective model based on first-principles calculations of the intermolecular transfer integral.

RESULTS AND DISCUSSION

First of all, we study the interaction of one isolated P3HT chain with the ZnO surface, which is represented in Figure 1. We focus on the nonpolar (10̄10) surface because it is the most stable (i.e., the most likely to occur in real samples). It is known¹⁴ that, due to the good self-passivation of the ZnO surface, the interaction between the P3HT molecule and the ZnO surface is mainly physisorption. In vacuo and at low temperatures, we find that the P3HT molecule is physisorbed with a binding energy equal to

Received: February 10, 2011

Revised: March 25, 2011

Published: April 22, 2011

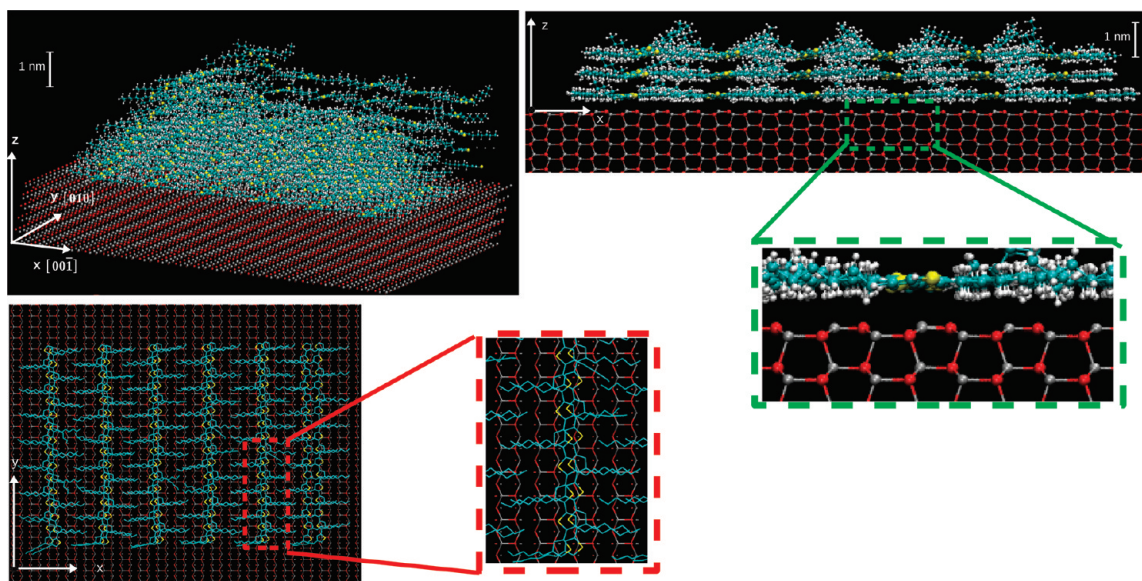


Figure 1. Perspective, lateral, and top views of the system A relaxed on the ZnO surface.

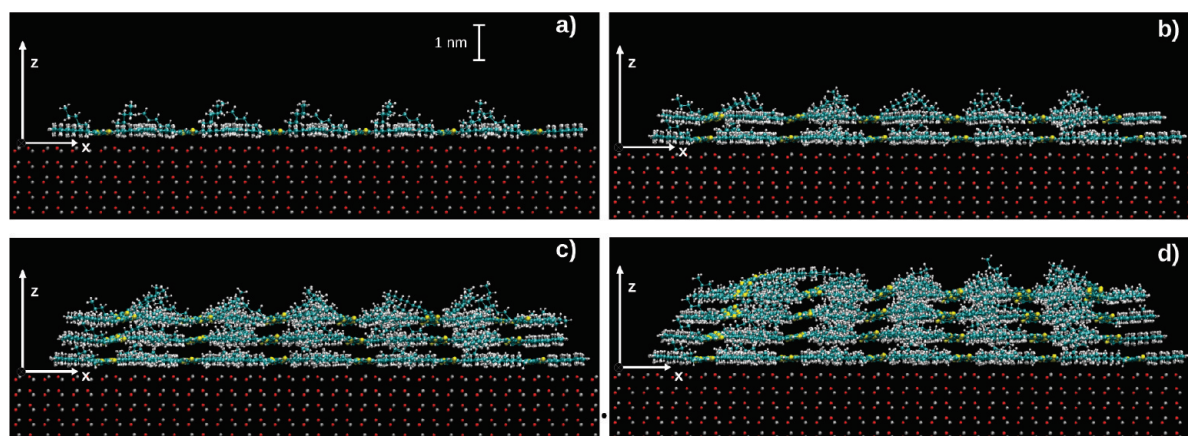


Figure 2. Assembling of P3HT layers on the ZnO surface.

0.57 eV per monomer, mostly due to dispersive and electrostatic interactions. In the bound configuration, the backbone of the molecule is aligned to the [010] crystallographic direction (y axis in Figure 1) along the rows (hereafter, named channels) formed by the ZnO dimers of the surface (see Figure 1). The thiophene rings of the backbone are found parallel to the surface. The binding of the molecule on the surface is driven by the interaction between the positively charged zinc atoms of the surface and the negatively charged carbon atoms of the aromatic ring. The sulfur atoms, in turn, are practically neutral, consistent with DFT calculations.¹⁵ The backbone of the molecule, in its bound state, is nearly planar; distortions are basically found in the hexyl chains only. An almost isoenergetic binding occurs also when the backbone of the molecule is rotated by 90° along the [100] direction, but in this case, the corresponding P3HT/ZnO charge transfer has been found to be inefficient.¹⁴ Accordingly, in the photovoltaic perspective, we focus on the [010] alignment of the polymer on ZnO.

Concerning the crystalline structure of the polymer, it is known¹⁵ that P3HT has two phases with similar energies: the *aligned* one, where the thiophene rings of two stacked molecules

are perfectly aligned on top of each other, and the *staggered* one, where the molecules are shifted by one thiophene unit along the backbone. The best transport properties are found in the aligned phase.^{14,15} Accordingly, aligned P3HT crystals are discussed in the present study. On the other hand, the metal oxide morphology is critical for the transport properties.¹⁶ In addition, the curvature of the ZnO substrate can affect the polymer organization and its adhesion energy, as found in P3HT/TiO₂ systems.¹⁷ Nevertheless, in order to study the intrinsic properties of the interface, here, we focus on the ideal case of a ZnO planar substrate.

An example of the hybrid interfaces generated in the present investigation is reported in Figure 1. It consists of a portion of the P3HT nanocrystal with dimensions of 10 nm × 5 nm × 2 nm on the crystalline ZnO (10̄10) surface. Typical microcrystalline P3HT domains in real samples have dimensions as small as 10–50 nm.¹⁵ Each polymer nanocrystal of our models is formed by 30 molecules with a length of 5 nm (16 monomers).

Because the polymer microstructure is highly sensitive to the synthesis conditions,¹⁸ we use two different methods to generate the hybrid interfaces: (i) assembling (A), where the nanocrystal

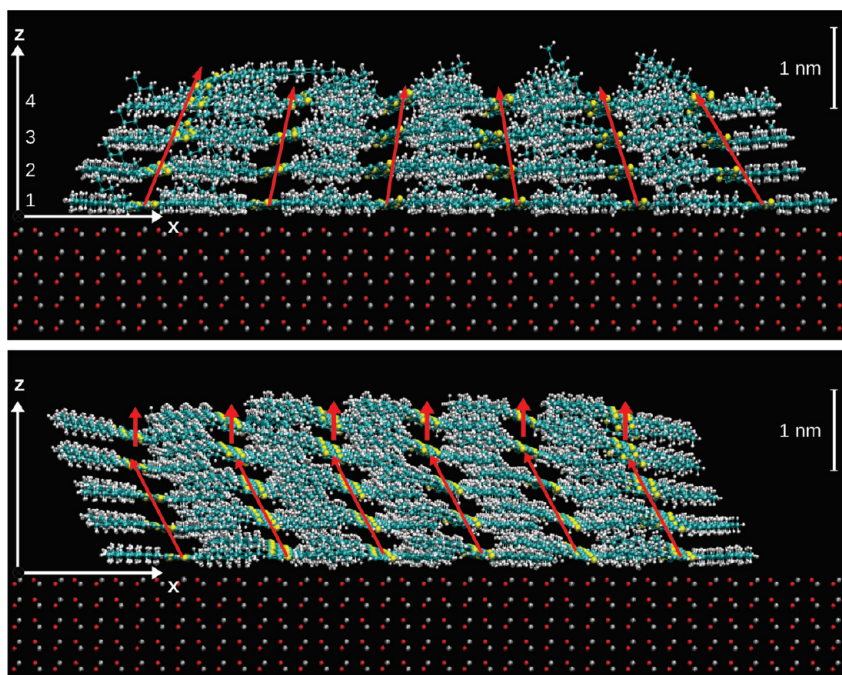


Figure 3. Final configuration of the system A (upper panel) and M (lower panel) on the ZnO surface. The red arrows represent the direction of the charge carriers.

is assembled layer by layer on the ZnO surface, and (ii) merging (M), where a polymer nanocrystal previously formed and the ZnO surface are merged. By comparing the results in both cases, we control the morphology dependence on the initial polymer configurations.

The atomistic models generated during the assembling procedure (A) are reported in Figure 2. Each P3HT layer consists of six chains with backbones along the y direction. It is known that, in vacuo, when a substrate is present, the polymer chains tend to organize into layers named *s*-foils,¹⁵ as the ones represented in panel (a) of Figure 2. *s*-foils are likely to form because the molecule/substrate adhesion (~ 0.6 eV/monomer) is larger than the polymer/polymer cohesion (~ 0.1 eV/monomer).¹⁵ Accordingly, in ideal conditions, the P3HT molecules tend to cover the surface by forming a monolayer. The interdigitation distance a between P3HT molecules within the *s*-foil along the x direction is calculated to be $a \sim 16.4$ Å. This is larger than the interdigitation distance $a_0 = 15.8$ Å in crystalline P3HT. Because the molecules tend to stay along surface channels, we attribute such a deviation to the mismatch of the polymer lattice spacing with the ZnO channels interdistance $l = 5.47$ Å. In fact, it turns out that $a \sim 3l$, that is, the smallest multiple of l that best matches a_0 . Because $a > a_0$, the *s*-foil at the ZnO surface is tensile-strained along the x direction. A large decrease of the spacing is observed within the second layer corresponding to $a \sim 15$ Å. Notably, this value is smaller than a_0 . Also the $\pi-\pi$ distances along z are increased with respect to the perfect crystal. The interdigitation distance further decreases within subsequent layers at larger distances from the ZnO surface. Finally, we found that, as the number of layers increases, there is a tendency of the hexyl chains to deviate from the ideal planar geometry. Accordingly, the polymer disorder increases with the number of layers.

Lattice mismatch effects are also observed at the M interface. In this case, a P3HT nanocrystal (with the same dimension as in the A model) is put on the ZnO surface at 7 Å and relaxed. The interdigitation distance within the first foil is found to be $3l$ and $2l$

alternatively. The corresponding average value is $2.5l \sim 13.7$ Å, corresponding to a compressive strain. At variance with the A model, the interdigitation distance does not change sizeably while moving to foils at larger distances from the interface.

The relaxed A and M interfaces are reported in Figure 3. In both cases, the order (for example, the stacking of thiophenes) is reduced by the presence of the substrate. In a perfect crystalline polymer, the thiophene rings give rise to $\pi-\pi$ channels where holes can hop easily from one molecule to the other. In both A and M models, the polymer $\pi-\pi$ channels (indicated in Figure 3 by red arrows) are affected by disorder and they are not orthogonal to the substrate. Such morphological features are expected to modify the transport properties of the polymer. For example, in the case of a crystalline polymer, the carriers can easily go close or move away from the interface, provided that the channels are orthogonal to the substrate. This corresponds to the most favorable case for photovoltaic efficiency: on the one hand, excitons that are generated within the polymer can easily diffuse toward the interface in order to be separated; on the other hand, carriers generated at the interface (as a result of exciton dissociation) can easily move away from the interface before recombining. In the opposite case, when the $\pi-\pi$ channels are parallel to the interface or when the polymer is disordered, the carriers cannot easily move away from the interface. In conclusion, for transport and performances, the order in the direction normal to the interface is a key property. To analyze quantitatively the stacking and transport properties, we introduce first of all the concept of effective area. The idea is to represent each thiophene ring by an elliptical shape in the plane of the molecule (see the inset of Figure 4). We then calculate the projected overlap area Θ^\perp (in the normal $x-y$ plane) between pairs of neighboring molecules along z . This quantity is related to the crystalline order of the system, and it is small in disordered or amorphous polymer films. In particular, Θ^\perp is maximum when the thiophenes of two neighboring molecules are perfectly aligned and parallel to the $x-y$ plane. Conversely, Θ^\perp is smaller when thiophenes are shifted

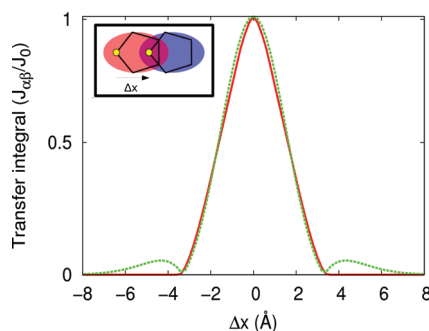


Figure 4. Comparison between the relative transfer integral $J_{\alpha\beta}/J_0$ as computed approximating thiophene rings by ellipses (solid line) and first-principles calculations (dashed line).

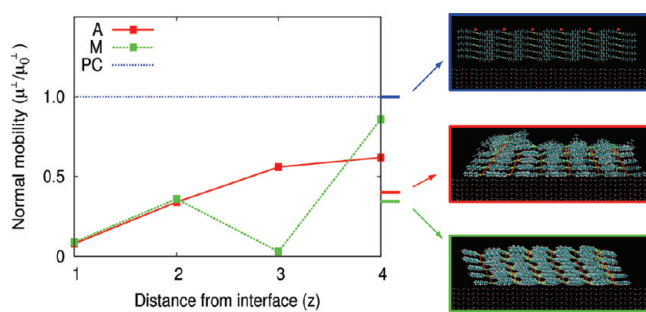


Figure 5. Normal mobility obtained by approximating the thiophene rings with ellipses with an eccentricity of $\epsilon = 1.15$.

in the x or y direction or when the molecules are tilted with respect to z . We demonstrate below that Θ^\perp can be used to calculate the polymer mobility normal to the interface.

If we refer to the Marcus theory,^{19,20} the mobility μ in the polymer is given considering the local probability $k_{\alpha\beta}$ that a hole hops between neighboring molecules, α and β .²¹ $k_{\alpha\beta}$, for a fixed temperature, is proportional to $J_{\alpha\beta}^2$, where $J_{\alpha\beta}$ is the transfer integral between the molecular electronic orbitals.²² $J_{\alpha\beta}$ depends on the relative position and orientation of the two molecules. We calculate $J_{\alpha\beta}$ from first-principles (see the Method section) for the case of two infinite thiophene chains oriented along the y direction and stacked along z . In Figure 4, we report the $J_{\alpha\beta}$ dependence on the relative x shift of the two chains with respect to the dependence of the transfer integral J_0 calculated at the equilibrium distance d_0 . The maximum $J_{\alpha\beta}$ is found at zero shift (i.e., maximum overlap area), and by increasing x up to $x = 3.6$ Å, it decreases monotonically to zero. In the same figure, we report the stacking parameter Θ^\perp calculated by using ellipses with an eccentricity of $\epsilon = 1.15$, chosen so as to best fit the first-principles calculations. Small differences (few percents) are found only at shifts of 4–6 Å, but the overall agreement is good.

As for the $J_{\alpha\beta}$ dependence on the $\pi-\pi$ distance d between the two molecules, we use $(J_{\alpha\beta}/J_0) = \exp(-\gamma(d - d_0)/d_0)$,²¹ where γ is a fitting parameter. By using two dithiophenes, we find that $d_0 = 3.9$ Å, $J_0 = 0.1755$ eV, and $\gamma = 6.5$. Accordingly, $J_{\alpha\beta}$ has a strong dependence on the $\pi-\pi$ distance; for example, for deviations from d_0 as small as 5%, the integral $J_{\alpha\beta}$ is affected by 30%. In conclusion, the stacking parameter Θ^\perp can be used as a good approximation for the $J_{\alpha\beta}$ dependence on x shifts.

When the above results are combined, $J_{\alpha\beta}$ can be calculated for any relative position and orientation of the two molecules. The local

contribution for the mobility in the direction normal to the interface, μ^\perp , can be calculated from the knowledge of the overlap Θ^\perp

$$\frac{\mu^\perp}{\mu_0^\perp} = e^{-2\gamma \left(\frac{d - d_0}{d_0} \right)} \left(\frac{\Theta^\perp}{\Theta_0^\perp} \right)^2 \quad (1)$$

where μ_0^\perp and Θ_0^\perp are, respectively, the mobility and the effective overlap in the perfect P3HT crystal.

Equation 1 can be used to calculate the average normal mobility within polymer layers as a function of the distance from the interface, as shown in Figure 5, where the numbering of the layers corresponds to that of Figure 3. Notably, the two models have identical normal mobilities at the first two layers, corresponding to a reduction with respect to the perfect crystal (PC). In the case of the M model, an open-circuit-like behavior (a strong increase of the resistivity) is observed at $z = 3$, where a kink in the π channels is observed. At larger distances, the mobility increases toward the crystalline value. We find that the average mobility is reduced by a factor of 2.5 (3) in the A (M) model.

We conclude that polymer chains likely misaligned close to the ZnO surface, thus reducing the normal carrier mobility in the first layers. Holes that are generated at the interface are not able to diffuse through the polymer, and as a consequence, they likely recombine with electrons. Similarly, excitons photogenerated within the polymer cannot easily move to the interface in order to be separated.

Present models have been obtained under ideal conditions. We expect that thermal fluctuations, or the presence of the solvent or other chemical impurities, can further reduce the order at the interface. Accordingly, the calculated mobility represents an upper limit for realistic interfaces. Our conclusions are consistent with experimental findings, suggesting the formation of disordered polymer at the interface.¹⁰

In conclusion, the ZnO interface affects dramatically the local mobility of the polymer close to the interface. We expect that, by improving the lattice matching of the polymer/substrate (e.g., by modifying the polymer hexyl chains or by using different metal oxides or suitable molecules), the crystallinity and the mobility at the interface can be, in principle, improved by a factor of 2 or more.

METHOD

For each interface model, we perform MD simulations consisting of low-temperature annealings (0.1 ns at 1 K), followed by atomic forces relaxations based on a standard conjugated gradients algorithm. Such low temperatures are considered in order to explore the most favorable conditions for crystalline order.

Because of the large number of atoms (~ 25000), we calculate interatomic forces by using model potentials. Interactions within ZnO are described as the sum of Coulomb and a Buckingham-type two-body potential.²³ As for P3HT, we adopt the AMBER force field,²⁴ including both bonding (bonds, bending, torsional) and nonbonding (van der Waals plus Coulomb) contributions. For hybrid ZnO/P3HT interactions, we use a sum of Coulomb and Lennard-Jones contributions.¹⁷ Simulations were performed by the DL_POLY 3.09 code.²⁵ The velocity Verlet algorithm with a time step of 1.0 fs is used to solve the equations of motion. A mesh Ewald algorithm²⁶ was used for the long-range electrostatic forces, and the van der Waals interactions were cutoff at 9.5 Å.

First-principles calculations for the transport properties were performed within the density functional theory (DFT) level. The estimate of the electronic coupling for cofacial dimers was obtained using the so-called “energy splitting in dimer” method.²² In this

method, the transfer integral for holes can be computed evaluating the energy difference between the orbitals resulting from the overlap of the highest occupied molecular orbitals of the two interacting molecules: $J_{\alpha\beta} = (\varepsilon_{\text{HOMO}} - \varepsilon_{\text{HOMO-1}})/2$, where $\varepsilon_{\text{HOMO}}$ and $\varepsilon_{\text{HOMO-1}}$ are the energies of the two highest occupied molecular orbitals of the dimer. We used the gradient-corrected PBE density functional²⁷ together with a plane-wave basis set and ultrasoft pseudopotentials as implemented in the CPMD²⁸ program package; to account for dispersion interactions, we used the empirical dispersion correction proposed by Grimme,²⁹ which adds a van der Waals-type term scaling as R^{-6} into the total energy of the system.

AUTHOR INFORMATION

Corresponding Author

*E-mail: misaba@dsf.unica.it (M.I.S.), alessandro.mattoni@dsf.unica.it (A.M.).

ACKNOWLEDGMENT

This work has been funded by the Italian Institute of Technology (IIT) under Project SEED “POLYPHEMO” and Regione Autonoma della Sardegna under Project “Design di nanomateriali ibridi organici/inorganici per l’energia fotovoltaica” L.R.7/2007. We acknowledge computational support by CYBERSAR (Cagliari, Italy), CASPUR (Rome, Italy) and CINECA (Casalecchio di Reno, Italy).

REFERENCES

- (1) Hsu, J. W.; Lloyd, M. T. *MRS Bull.* **2010**, *422*, 234701.
- (2) Mayer, A.; Scully, S.; Hardin, B.; Rowell, M.; McGehee, M. *Mater. Today* **2007**, *10*, 28–33.
- (3) Sirringhaus, H.; Brown, P.; Friend, R.; Nielsen, M.; Bechgaard, K.; Langeveld-Voss, B.; Spiering, A.; Janssen, R.; Herwig, E. M. P.; de Leeuw, D. *Nature* **1999**, *401*, 685–688.
- (4) Cho, S.; Lee, K.; Yuen, J.; Wang, G.; Moses, D.; Heeger, A.; Surin, M.; Lazzaroni, R. *J. Appl. Phys.* **2006**, *100*, 114503.
- (5) Sheng, C.; Tong, M.; Singh, S.; Vardeny, Z. V. *Phys. Rev. B* **2007**, *75*, 085206.
- (6) Özgür, U.; Alivov, Y. I.; Liu, C.; Teke, A.; Reshchikov, M. A.; Doðan, S.; Avrutin, V.; Cho, S.-J.; Morkoç, H. *J. Appl. Phys.* **2005**, *98*, 041301.
- (7) Lincot, D. *MRS Bull.* **2010**, *3*, 778–788.
- (8) Oosterhout, S. D.; Wienk, M.; van Bavel, S. S.; Thiedmann, R.; Koster, L. J. A.; Gilot, J.; Loos, J.; Schmidt, V.; Janssen, R. A. J. *Nat. Mater.* **2009**, *8*, 818–824.
- (9) Cai, W.; Gongn, X.; Cao, Y. *Sol. Energy Mater. Sol. Cells* **2010**, *94*, 114–127.
- (10) Lloyd, M. T.; Prasankumar, R. P.; Sinclair, M. B.; Mayer, A. C.; Olson, D. C.; Hsu, J. W. P. *J. Mater. Chem.* **2009**, *19*, 4609–4614.
- (11) Spano, F. *J. Chem. Phys.* **2005**, *122*, 234701.
- (12) Veres, J.; Ogier, S.; Lloyd, G.; de Leeuw, D. *Chem. Mater.* **2004**, *16*, 4543–4555.
- (13) Kline, R.; McGehee, M.; Toney, M. *Nat. Mater.* **2006**, *5*, 222–228.
- (14) Dag, S.; Wang, L.-W. *Nano Lett.* **2008**, *8*, 4185–4190.
- (15) Melis, C.; Colombo, L.; Mattoni, A. *J. Phys. Chem. C* **2010**, *115*, 576–581.
- (16) Galoppini, E.; Rochford, J.; Chen, H.; Saraf, G.; Lu, Y.; Hagfeldt, A.; Boschloo, G. *J. Phys. Chem. B* **2006**, *110*, 16159–16161.
- (17) Melis, C.; Mattoni, A.; Colombo, L. *J. Phys. Chem. C* **2010**, *114*, 3401.
- (18) Zhao, K.; Xue, L.; Liu, J.; Gao, X.; Wu, S.; Han, Y.; Geng, Y. *Langmuir* **2010**, *26*, 471–477.
- (19) Marcus, R. *Rev. Mod. Phys.* **1993**, *65*, 599–610.
- (20) Rühle, V.; Kirkpatrick, J.; Andrienko, D. *J. Chem. Phys.* **2010**, *132*, 134103.
- (21) Lan, Y.-K.; Yang, C. H.; Yang, H.-C. *Polym. Int.* **2010**, *59*, 16–21.
- (22) McClure, S.; Buriak, J. M.; DiLabio, G. *J. Phys. Chem. C* **2010**, *114*, 10952–10961.
- (23) Moon, W. H.; Hwang, H. *J. Nanotechnology* **2008**, *19*, 225703.
- (24) Ponder, J.; Case, D. *Adv. Protein Chem.* **2003**, *66*, 27–85.
- (25) Todorov, I.; Smith, W.; Trachenko, K.; Dove, M. *J. Mater. Chem.* **2006**, *16*, 1911–1918.
- (26) Essmann, U.; Perera, L.; Berkowitz, M.; Darden, T.; Lee, H.; Pedersen, L. *J. Chem. Phys.* **1995**, *103*, 8577–8593.
- (27) Perdew, J. P.; Burke, K.; Ernzerhof, M. *Phys. Rev. Lett.* **1996**, *77*, 3865–3868.
- (28) CPMD, V3.9; IBM Corp, 1990–2001, MPI für Festkörperforschung Stuttgart, 1997–2001.
- (29) Grimme, S. *J. Comput. Chem.* **2006**, *27*, 1787–1799.